# Iron conservation by reduction of metalloenzyme inventories in the marine diazotroph *Crocosphaera watsonii*

Mak A. Saito[a,1], Erin M. Bertrand[a], Stephanie Dutkiewicz[b], Vladimir V. Bulygin[a,2], Dawn M. Moran[a], Fanny M. Monteiro[b], Michael J. Follows[b], Frederica W. Valois[c], and John B. Waterbury[c]

[a]Marine Chemistry and Geochemistry Department and [c]Biology Department, Woods Hole Oceanographic Institution, Woods Hole, MA 02543; and [b]Earth Atmospheric and Planetary Sciences Department, Massachusetts Institute of Technology (MIT), 77 Massachusetts Avenue, Cambridge, MA 02139

The marine nitrogen fixing microorganisms (diazotrophs) are a major source of nitrogen to open ocean ecosystems and are predicted to be limited by iron in most marine environments. Here we use global and targeted proteomic analyses on a key unicellular marine diazotroph *Crocosphaera watsonii* to reveal large scale diel changes in its proteome, including substantial variations in concentrations of iron metalloproteins involved in nitrogen fixation and photosynthesis, as well as nocturnal flavodoxin production. The daily synthesis and degradation of enzymes in coordination with their utilization results in a lowered cellular metalloenzyme inventory that requires ∼40% less iron than if these enzymes were maintained throughout the diel cycle. This strategy is energetically expensive, but appears to serve as an important adaptation for confronting the iron scarcity of the open oceans. A global numerical model of ocean circulation, biogeochemistry and ecosystems suggests that *Crocosphaera*'s ability to reduce its iron-metalloenzyme inventory provides two advantages: It allows *Crocosphaera* to inhabit regions lower in iron and allows the same iron supply to support higher *Crocosphaera* biomass and nitrogen fixation than if they did not have this reduced iron requirement.

cyanobacteria | marine iron cycle | nitrogen cycle

The biological fixation of atmospheric dinitrogen into ammonia has a major impact on the extent of marine primary production (1, 2). Only a small number of bacteria are known to contribute to nitrogen fixation in open ocean environments, and they typically comprise a tiny fraction (<0.1%) of the overall microbial community (3, 4). Among these, the unicellular diazotroph *Crocosphaera watsonii* is estimated to be a significant contributor to oceanic nitrogen fixation (4–6). Whereas much of the primary productivity in the tropical and subtropical regions of the oceans is predicted to be nitrogen limited, the diazotrophs' nitrogen source, resupplied from the large atmospheric reservoir, is essentially limitless. Instead, iron is considered the critical micronutrient for marine diazotrophs due to their use of the iron-nitrogenase protein complex containing a homodimeric iron protein with a 4Fe:4S metallocluster (NifH) and a heterotetrameric molybdenum-iron protein with an 8Fe:7S P cluster and a 7 Fe and 1 Mo MoFe cofactor (NifDK, α and β subunits) (7, 8) (Table S1). Field experiments and models both predict the distribution of oceanic nitrogen fixation to be primarily constrained by the availability of iron (2, 9–11). Despite this importance of iron on marine nitrogen fixation, there is a limited understanding of how marine diazotrophs have adapted to this low iron environment (12–17).

The coexistence of oxygenic photosynthesis and nitrogen fixation metabolisms presents a unique challenge for diazotrophs due to their high iron demands and the chemical incompatibility of molecular oxygen and the nitrogenase protein complex. Previous elemental studies measuring whole cell iron content in *Crocosphaera* found increased iron during the dark period when nitrogen fixation is occurring (15). Whereas this finding was consistent with theoretical studies predicting a large iron requirement in marine diazotrophs (13, 18), it has been somewhat controversial due to the implication of a dynamic yet poorly understood diel cycle for intracellular iron. Several unicellular diazotrophs, including *Crocosphaera watsonii*, have been observed to fix nitrogen during the dark period (Fig. 1*A*), and this is widely viewed as an adaption for temporal separation of photosynthesis and nitrogen fixation to avoid the oxygen disruption of the nitrogenase complex (6, 19, 20). Global transcriptional studies have also observed large scale changes in the transcriptomes of the unicellular diazotrophs *Crocosphaera watsonii* (21), *Cyanothece* (22), *Gloeothece* (23), and a hot-spring *Synechococcus* (24) during the diel cycle, consistent with a temporal separation of photosynthesis and nitrogen fixation. Yet the possibility that diel cycling of the transcriptome or proteome might affect the iron requirement has not been previously discussed, likely because transcriptional studies provide information about gene expression rather than actual enzyme inventories, and immunological protein studies thus far, while having detected diel oscillations of the NifH subunit in *Crocosphaera* and *Gloeothece* (23, 25), are limited to a few select proteins with no global or absolute quantitative proteome studies of diazotrophs published as of yet. As a result, it has remained uncertain whether the observed diel transcriptome cycling was needed for the maintenance of a relatively consistent proteome or was in fact causing large changes in the global proteome composition during each diel cycle.

Recent advances in proteomic technologies hold promise for elucidating mechanistic connections between the biochemistry of important microbes and global biogeochemical cycles. There are two broad approaches to mass spectrometry based proteomics: global shotgun proteomic approaches that can semiquantitatively survey the relative abundance of hundreds of proteins simultaneously using spectral counting (26), and targeted approaches that use selected reaction monitoring (SRM) mass spectrometry with isotopically labeled peptide standards for absolute quantification of proteins of interest (27). Though there are several culture-based studies of marine microbes (26, 28) and field assessments of abundant proteins (29, 30), the combined application of global and targeted proteomic approaches to problems of
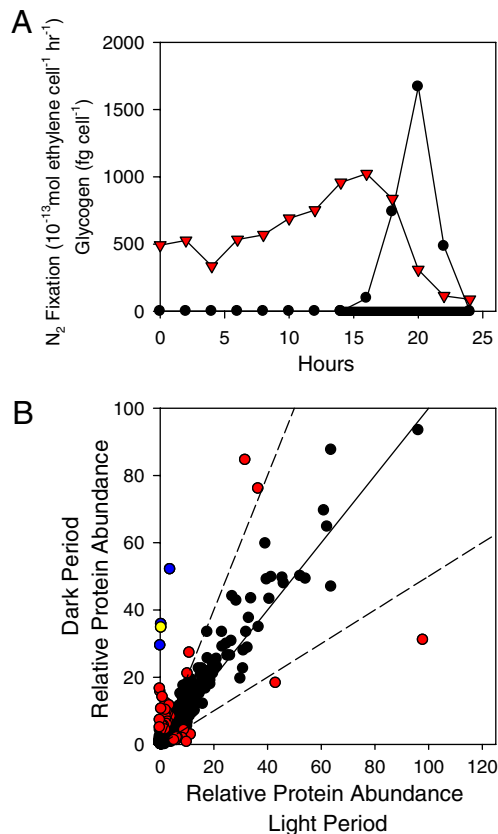
**Fig. 1.** Variations in the *Crocosphaera* proteome between the light and dark photoperiod. (*A*) Dark period nitrogen fixation (black) and glycogen storage (red) during a diel cycle (dark, black bar). (*B*) Relative protein abundance during light and dark periods, where similar expression (solid line, black circles; also see Fig. S1*A* for comparison of technical replicates) is contrasted by a number of proteins (colors), including the nitrogenase complex metalloenzymes (blue) and flavodoxin (yellow), with greater than 2-fold change in relative abundance (dashed lines) above a threshold of 5 normalized spectral counts in at least one treatment. Data are mean of six technical replicates.



**Fig. 2.** Cluster analysis of global proteome during the diel cycle. Color indicates higher (yellow) or lower (blue) relative abundance relative to the centered mean value (black). Horizontal axis is hours from onset of light (L) or dark (D) period. Proteome data was filtered for proteins with at least three time points having greater than 10 spectral counts and a difference between maximum and minimum signals ≥14 spectral counts, prior to log transformation and normalization. Two major clusters were observed corresponding to the light and dark photoperiods.

marine biogeochemical relevance, such as the iron limitation of marine diazotrophy, has not yet been reported.

## Results and Discussion

The diel cycle and inventory of iron metalloenzymes in *Crocosphaera watsonii* were investigated using global and targeted liquid chromatography mass spectrometry (LC-MS) proteomic techniques from three distinct culture experiments all grown on a 14:10 light:dark cycle: a day-night experiment sampled during the light and dark photoperiod (sampled 10 h from lights on and 7 h from lights off) analyzed for global proteome using both 1D and 2D LC-MS approaches, a time course study (diel hereon) sampled every 2–3 h for 30 h (beginning 4 h from lights on) and analyzed for global proteome using 1D LC-MS and for absolute quantities of targeted proteins, and a set of biological triplicate cultures (sampled 6.5 h into light period, and 3 and 6 h into the dark period) analyzed for targeted protein abundances by mass spectrometry.

Of the 477 unique proteins identified in the global proteomic 1D analysis of the day-night experiment [0.65% false positive rate (FPR) (31)], 37 proteins were found to have a 2-fold or greater change in abundance between the day and night (Fig. 1*B*). These results were confirmed in the deeper 2D chromatography proteome where 160 of the 1,108 identified proteins (0.11% FPR) showed a greater than 2-fold change (Fig. S1*B*). A time course of the diel cycle clearly showed a cycling of protein abundance (Fig. 2), where 100 proteins were found to be above a threshold
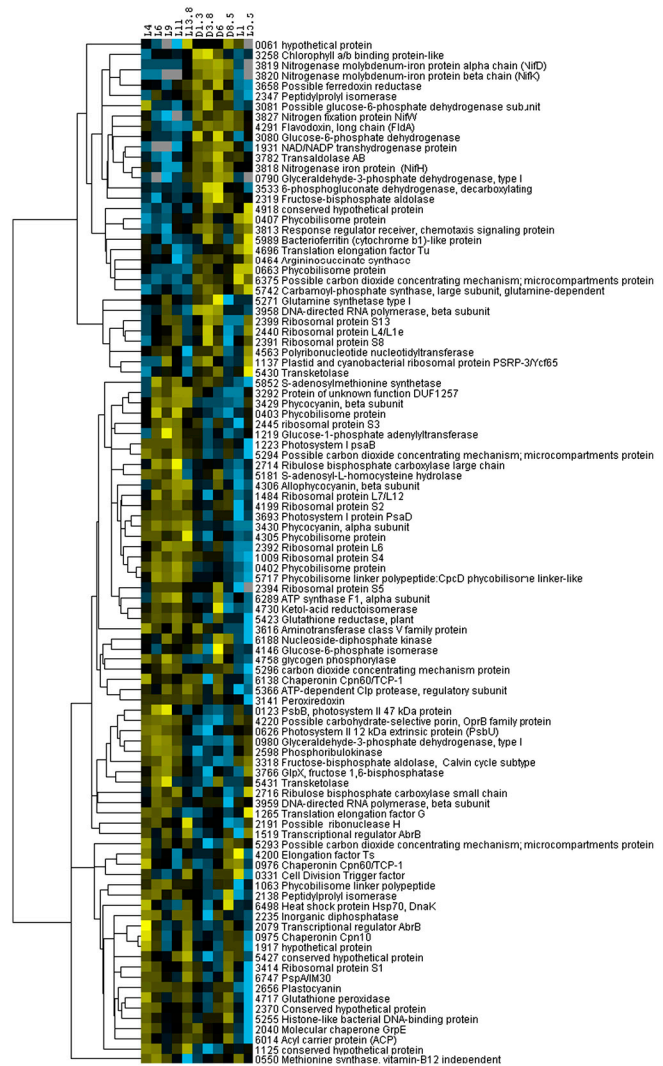
spectral count signal (≥10) and displayed a diel variation in amplitude (max - min ≥ 14). Cluster analysis revealed two major groups that include key photosystem or nitrogen fixation proteins with increased abundances during the day and night respectively. These experiments demonstrate that the diel cycling observed in the transcriptome of unicellular diazotrophs (21, 22, 32) manifests itself in large scale changes in the global proteome, where more than 20% of the measured proteins in the diel experiment showed diel variation. In both the day-night and diel experiments, the metalloenzymes involved in nitrogen fixation in *Crocosphaera watsonii* were among those with the most pronounced changes in abundance, being largely absent during the day and present at night (Figs 1*B* and 2, Fig. S2, and Dataset S1).

Based on these global experiments, the absolute abundances of nine protein targets in the diel experiment were determined by triple quadrapole SRM mass spectrometry using isotopically labeled internal standards (Table S2). The abundance of the three nitrogenase metalloproteins ranged from nondetectable levels during the photoperiod to being among the most abundant pro-

teins in the proteome in the dark period (Fig. 3 *A–C*). At their peak abundances, the ratio of the iron protein to molybdenum-iron protein subunits (α used here) was 3.5:1, consistent with previous observations of a 3:1 cellular ratio (23) and a 2:1 stoichiometry within the nitrogenase protein complex (33). Together these global and targeted proteome measurements provide evidence for the nocturnal synthesis of the metalloenzymes in the nitrogenase complex followed by their complete diurnal degradation.

Flavodoxin was observed to increase in abundance during the dark period (Fig. 3*D*), similar to the nitrogenase metalloenzymes and in contrast with the increased flavodoxin abundances observed in most phytoplankton under iron deprivation (34). This suggests the ferredoxin-flavodoxin substitution for electron transport in photosynthesis does not occur appreciably in *Crocosphaera*. The global proteome of a short-term iron deprivation experiment was sampled during the light photoperiod to allow differentiation of iron effects from the dark expression. No increase in flavodoxin in response to iron stress was observed 24 h after the addition of an exogenous siderophore (Fig. S1 *C–F*), consistent with the hypothesis that flavodoxin could be functioning as an electron carrier for nitrogenase instead of ferredoxin (35). The use of flavodoxin at night even under iron replete conditions appears to be an adaptation for the overall minimization of the cellular iron demand in this microbe.

In a mirror image of the nitrogenase metalloenzymes and flavodoxin, numerous proteins were more abundant during the photoperiod (Figs. 1*B* and 2). In particular, several proteins from iron-rich photosystem I decreased during the dark period and increased during light period, including PsaA, PsaB, PsaD, and PsaF (PsaA and PsaB shown in Fig. 3 *E* and *F*). The iron-containing cytochromes b6 and c550 were among the most abundant cytochromes detected by spectral counting (f, P450, and b559 and c oxidase were also detected) and showed large decreases in abundance during the dark period as measured by targeted mass spectrometry (Fig. 3 *G* and *H*; 2- and 15-fold respectively). The degradation of substantial quantities of cytochrome b6 and c550 should release a number of iron-containing hemes during the dark period. Two heme oxygenases, which are capable of liberating iron from heme, were identified in the proteome, showed diel variations, and may be important in iron recycling (Fig. S2). Iron storage bacterioferritin proteins were also identified in the proteome, one of which showed some diel periodicity (Fig. S2). Diel cycling is not necessarily expected for bacterioferritin given that iron is thought to be added and removed from the ferritin cage without its degradation.

These results portray a *Crocosphaera* proteome that is dynamic, shifting its metalloenzyme inventory to suit the alternating temporal needs of nitrogen fixation and photosynthetic biochemical activity. Whereas *Crocosphaera*'s distinct nocturnal nitrogenase activity is one of its defining characteristics in both laboratory
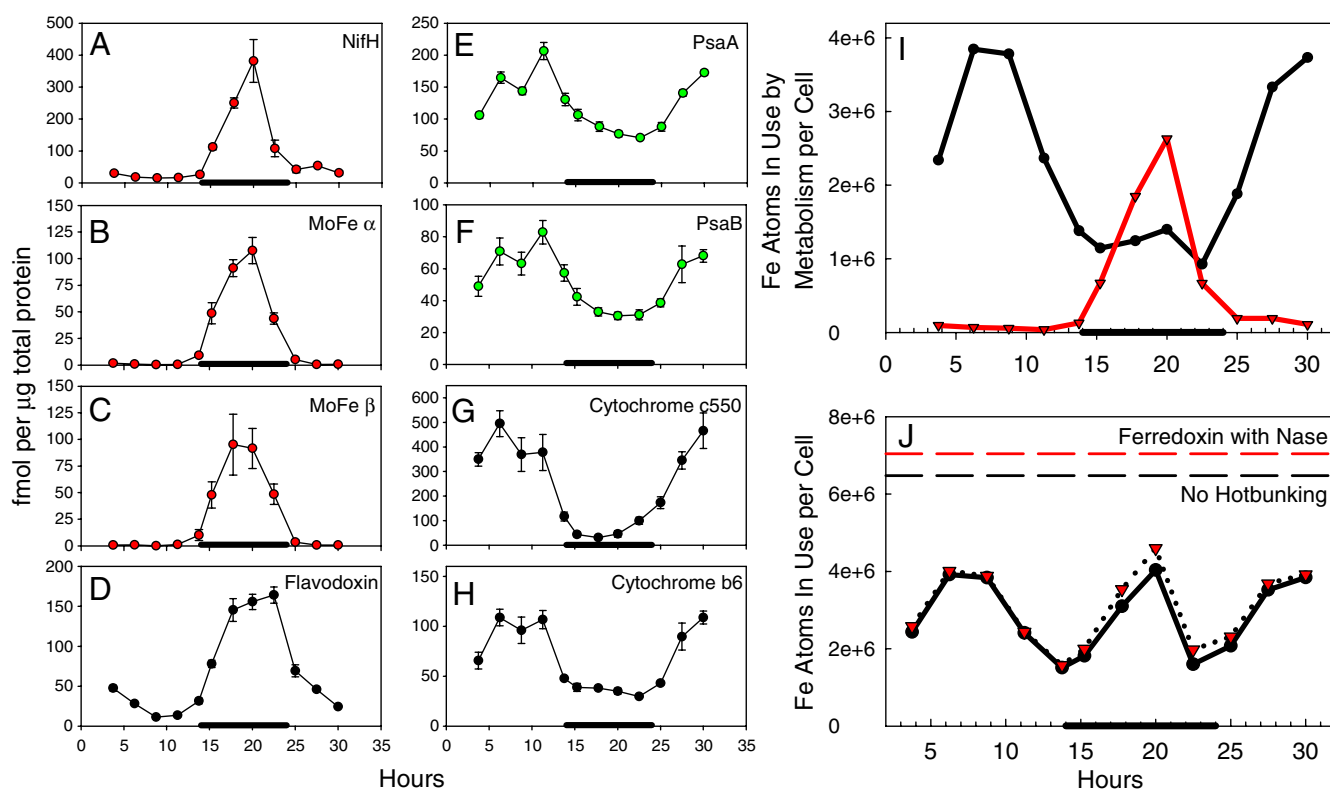
**Fig. 3.** Absolute quantitation of nitrogenase metalloproteins and selected photosynthesis and electron transport proteins during the diel cycle, and estimates of cellular iron stoichiometry based on absolute protein concentrations. (*A–H*) Targeted proteomic analysis of iron-nitrogenase (NifH), molybdenum-iron protein subunits (NifDK, MoFe α, MoFe β), and flavodoxin, photosystem I proteins PsaA and PsaB, and cytochromes b6 and c550 during the diel cycle (darkness, black bar) as measured using SRM triple quadrapole liquid chromatography mass spectrometry employing isotopically labeled standards. Data are mean and one standard deviation of technical triplicates. (*I*) Iron demand associated with nitrogen fixation or photosynthesis estimated from protein abundances in *A–H*, total protein and cell concentrations, and metal enzyme stoichiometries (Fig. S3 and Table S1) assuming metalloenzymes were populated with iron (darkness, black bar). (*J*) Sum of photosynthesis and nitrogenase iron estimates in two scenarios (darkness, black bar): (*i*) the *Crocosphaera* hotbunking scenario summing the calculated values in panel *I* (black circles), and (*ii*) a hypothetical nonhotbunking scenario (dashed black line), where the maximum iron required for each process [the peak of each line in panel (*I*) is summed]. Two additional scenarios are shown, where measured flavodoxin is replaced by ferredoxin, assuming a conservative 1:1 substitution (hotbunking, red triangles; nonhotbunking, dashed red line). The hotbunking scenario represents an estimated 40% savings in iron through a reduction of the iron-metalloenzyme inventory involved with nitrogenase and photosynthesis.

and field studies (6, 36), the fate of the nitrogenase protein complex during the light period has remained controversial due to the technical limitations of transcriptional and immunological methods, where transcripts do not measure protein abundance and immunological methods may not detect posttranslationally modified proteins (6, 15, 21, 36, 37). Using mass spectrometry-based analysis of multiple tryptic peptides from each protein, this study demonstrates the near complete degradation of the metalloenzymes from the nitrogenase complex and the partial degradation of certain iron-containing components of photosynthesis. The extent of proteome cycling we observed in *Crocosphaera watsonii* was surprising given the potentially significant energetic cost. This proteome cycling likely serves the dual functions of preventing oxygen disruption to the nitrogenase complex as discussed previously (6, 19), as well as providing a mechanism for a significant reduction in metabolic iron demand. We argue that the latter is true based on stoichiometric calculations from the quantitative metalloenzyme data in Fig. 3 *A–H* and the associated iron stoichiometry for each metalloenzyme (Table S1). By summing the iron associated with major metalloenzymes, we calculated the amount of iron involved in nitrogen fixation and photosynthesis throughout the diel cycle (Fig. 3*I*). By degrading these metalloenzymes when they are not in use, *Crocosphaera* reduces its iron-metalloenzyme inventory for these metabolic functions at any given time by 38%, 40%, and 75% for peak night, peak day, and minimum, respectively, compared to a hypothetical situation where these metalloenzymes are not degraded (Fig. 3*J*). An additional experiment with targeted protein analyses on biological triplicates was consistent with these estimates of iron conservation from the diel experiment, using $45 \pm 19\%$ less iron during the photoperiod (6.5 h from lights on, $n = 3$), and $38 \pm 14\%$ and $38 \pm 22\%$ less iron during the dark period (sampled at 3 h and 6 h from lights off, $n = 3$ for each). These savings in iron use would be even larger if the iron-free flavodoxin observed during the dark period (Fig. 3*D*) was replaced by iron-requiring ferredoxin (Fig. 3*J*). Iron released by the degradation of these metalloenzymes could have several fates including storage in bacterioferritin or chaperones, loss from the cell, and reuse in other metalloenzymes. Given the severe iron limiting conditions of the upper oceans (2, 9), it seems likely that a fraction of this liberated iron inventory is participating in both nitrogen fixation and photosynthesis metabolic processes. This iron conservation strategy is analogous to the maritime practice of hotbunking, referring to ships that sail with more sailors (metalloenzyme requirements) than bunks (iron atoms), where sailors on opposing shifts share the same bunk—keeping the bunks continually hot (or iron atoms in use). Whereas it is methodologically difficult to document the sharing of individual iron atoms between metabolisms, our data clearly demonstrates the reduction in iron-metalloenzyme inventory and concurrent reduction in metabolic iron demand through diel proteome cycling (Fig. 3*J*).

Iron conservation by reducing the metalloenzyme inventory likely serves as a key component of a low iron marine niche for *Crocosphaera*. *Trichodesmium* sp. is another dominant oxygenic marine diazotroph that differs from *Crocosphaera* in that it fixes both nitrogen and carbon during the photoperiod (38, 39). As a result *Trichodesmium* sp. likely does not employ this iron conservation strategy to the extent used by *Crocosphaera*. This is consistent with reports of an approximately double cellular iron to carbon stoichiometry in *Trichodesmium* compared to *Crocosphaera* (>35 and $16 \pm 11$ $\mu$mol Fe mol $C^{-1}$, respectively) (14–16), as well as estimates of a large fraction of cellular iron being necessary for nitrogen fixation (22–50%) in *Trichodesmium* (13). A previous study of cellular iron in *Crocosphaera watsonii* observed an increase in iron concentrations per cell during the dark period (15). Our calculated iron per cell attributed to nitrogen fixation and photosynthesis are roughly consistent with measured values (15), and the higher iron content at night likely

results from diel proteome cycling with the added contributions of daytime uptake and accumulation of ferrous iron (21) produced by photochemical reduction (40) and photoperiod cell division (Fig. S4).

By reducing the nitrogen fixation and photosynthetic metalloenzyme inventory when each is not in use, *Crocosphaera watsonii* has evolved to require ~40% less iron than if these enzymes where maintained throughout the diel cycle (Fig. 3*J*). Though difficult to quantify, this process of resynthesizing enzymes every day must have an energetic expense. Based on our quantitative measurements, diel cycling of the three nitrogenase metalloproteins alone contributes ~2.3% of the total protein and all eight targeted proteins in Fig. 3 contribute 5.0% (using the difference between the maximum and minimum expression levels during the diel cycle). With many lower abundance proteins also undergoing diel cycling (Fig. 2), and with protein contributing roughly 40% of cellular biomass (41), these calculations provide some rough sense of the energetic cost for the increased protein synthesis required for this reduction in iron metabolic demand ("hotbunking" hereon). If *Crocosphaera watsonii* had evolved hotbunking from an ancestor that maintained its metalloenzymes through the diel, how would the trade-off between lower iron requirement and higher energetic cost affect where *Crocosphaera* would be competitive relative to its progenitor and other diazotrophs? A numerical global ocean circulation and ecosystem model (10, 42) is a useful tool to explore the implications of hotbunking on *Crocosphera's* habitat and nitrogen fixation rates in the global ocean. Our model resolves several phytoplankton types competing for resources, including analogs of several nondiazotrophs types, and unicellular and colonial marine diazotrophs, analogous to *Crocosphaera* and *Trichodesmium*, respectively. The modeled unicellular diazotrophs consist of two groups: a hypothetical control group that could not share cellular iron between photosynthesis and nitrogen fixation machinery (analogous to potential *Crocosphaera* ancestors that maintained their metalloenzyme inventory), and a hotbunking group (analogs of *Crocosphaera*, as suggested by this study) that are conferred with a lower cellular iron demand ($R$) at a cost to their growth rate ($\mu$):

$$\mu_H = \alpha\mu_C, \qquad R_H = \gamma R_c \quad \text{where } \alpha,\gamma < 1.$$

The subscript $H$ refers to hotbunkers and $C$ refers to the non-hotbunking control group. We conducted a suite of simulations with different assumptions of the trade-off between reduced growth and iron requirement, the respective values of $\alpha$ and $\gamma$. A larger value of $\alpha$ indicates less energetic cost, and a larger value of $\gamma$ indicates iron requirements closer to the control group.

Iron conservation strategies in *Crocosphera* provided an ecological advantage in the low iron environments of the open ocean (Fig. 4 and Fig. S5). The geographical habitat of the hotbunking-analogs extended further into iron-depleted water than both the hypothetical control group and the *Trichodesmium*-analogs. In simulations with favorable combinations of trade-offs (e.g., Fig. 4), the distribution of *Crocosphaera*-analogs is broadly consistent with those suggested by observations (4, 10). These simulation results are consistent with observations suggesting that *Trichodesmium* outcompetes *Crocosphaera* in areas with high iron (43). The extent of the hotbunking unicellular diazotoph habitat is strongly regulated by the trade-off assumed (Fig. 5 and Fig. S5). Predictably, if the energetic cost is too high, hotbunking is not a desirable trait. For large cost to growth (small $\alpha$) hotbunking diazotrophs do not survive (Fig. 5 *A* and *C*). On the other hand, for very little cost to growth (large $\alpha$) and a high reduction in iron requirement (low $\gamma$), the hotbunking diazotrophs outcompeted the control group and expand into even more oligotrophic regions (Figs. 4*C* and 5*B* and Fig. S5 *E* and *F*). Simulations with lower requirements for iron ($\gamma$ smaller) lead to a larger biomass of unicellular diazotrophs at any location than in a simulation
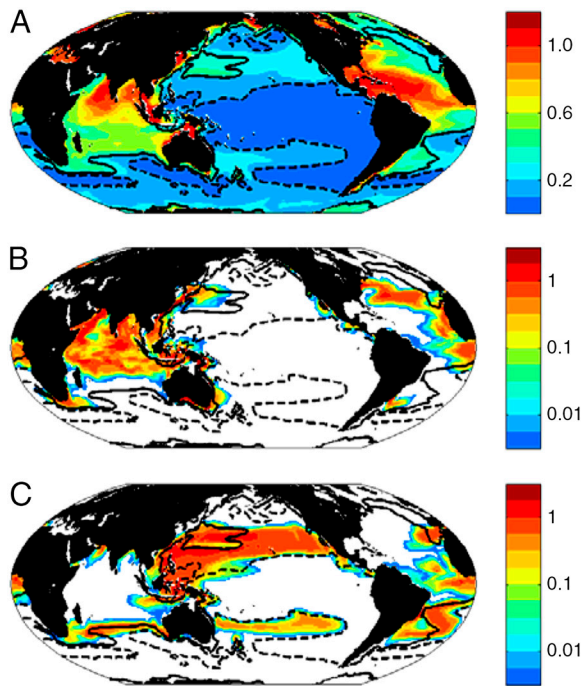
**Fig. 4.** Hotbunking unicellular diazotrophs inhabit waters with lower iron than the *Trichodesmium*-analogs and the unicellular control group (see Fig. S5) in the numerical simulations. Results are shown here for simulation where the hotbunking group have 90% of the growth rate and 60% the iron requirement of the control group ($\alpha = 0.9$, $\gamma = 0.6$, circle in Fig. 5). In this simulation the hotbunking diazotrophs outcompete the hypothetical control group everywhere. Annual mean model results for 0–50 m: (A) iron concentration (nM); (B) *Trichodesmium*-analogs (mgC m$^{-3}$); (C) hotbunking unicellular diazotrophs (mgC m$^{-3}$), analogs of *Crocosphaera watsonii*. Dashed and solid contours indicate 0.1 nM and 0.3 nM Fe respectively, and no shading (in *B* and *C*) indicates areas devoid of diazotrophs. The distribution of the diazotrophs is broadly consistent with those suggested by observations (4, 10). The model also includes analogs of several types of nondiazotrophic phytoplankton (diatoms, other large eukaryotes, *Prochlorococcus*, and other small phytoplankton). For less advantageous combinations of $\alpha$ and $\gamma$, the hotbunking group outcompete the control group only in the most iron-depleted regions (see Fig. 5 and Fig. S5).



**Fig. 5.** Results from a series of global circulation/ecosystem model numerical simulations with different assumptions on the trade-off between reduced growth and iron requirement (values of $\alpha$ and $\gamma$). (A) Area (10$^6$ km$^2$) inhabited by hotbunking unicellular diazotrophs. (B) Area (10$^6$ km$^2$) inhabited by the control nonhotbunking unicellular diazotrophs. (C) Global abundance of hotbunking unicellular diazotrophs (TgC). (D) Changes in global total nitrogen fixation (TgN/y). With increased $\alpha$ (a smaller cost to growth) and a decreased $\gamma$ (a lower requirement for iron) there are more regions where diazotrophy is supported, there is higher biomass of unicellular diazotrophs, and consequently higher total global autotrophic nitrogen fixation rates. If the energetic cost is low enough the hotbunking diazotrophs outcompete the control group everywhere (white regions of *B*). "Area" is calculated as the ocean surface area where the respective unicellular diazotrophs biomass is greater than 10$^{-3}$ mgC m$^{-3}$. Nitrogen fixation rate is calculated from all three types of diazotrophs included in the simulation (hotbunking unicellular diazotrophs, control group, and *Trichodesmium*-analogs). The circle denotes parameter values used for results shown in Fig. 4 and crosses for those in Fig. S5.

with higher $\gamma$; the same iron supply could support a higher biomass. Sharing cellular iron between photosynthesis and nitrogen fixation machinery allowed the model hotbunking diazotrophs to not only expand their habitat, but also to have higher biomass per mole of available iron. These two benefits of hotbunking lead to increased global unicellular diazotroph biomass than simulations that did not include this adaptation (Fig. 5*C*). As a consequence, total global nitrogen fixation increases between simulations with $\alpha$ and $\gamma$ combinations that shifted the population of unicellular diazotrophs from only control types to only hotbunking types (Fig. 5*D*). For the simulation shown in Fig. 4 (circles in Fig. 5) there was a 10% increase in global autotrophic nitrogen fixation relative to simulation with no hotbunkers (e.g., the white area of Fig. 5*A*). The overall affect of hotbunking on total global nitrogen fixation would be less than this value, because recent evidence demonstrates that heterotrophic nitrogen fixers also contribute significantly to marine nitrogen fixation (44).

Enzymes are agents for chemical transformations in the cycling of elements on Earth. Whereas genomic and transcriptional techniques can monitor the potential for enzyme synthesis, proteomic methods are now capable of their direct quantitation. Many require metals and hence reside at the intersection of coupled biogeochemical cycles. Our study demonstrates an application of proteomic technologies to study iron conservation in marine nitrogen fixation, where the important diazotroph *Crocosphaera* appears to have evolved a complex diel proteome
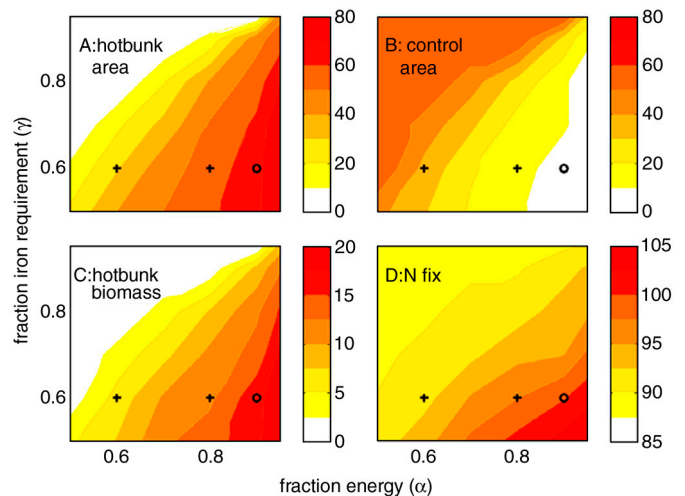
cycle that results in a reduction of iron-metalloenzyme inventory. The process elucidated by the molecular-level measurements described here appears to be of global importance. With rising atmospheric CO$_2$ suggested to cause increases in marine nitrogen fixation (45), as well as a potential decrease in iron availability to marine phytoplankton in general (46), understanding the biochemical adaptations for iron scarcity in diazotrophs and their implications for marine primary productivity will be of increasing importance.

## Methods

Axenic cultures of *Crocosphaera watsonii* were grown in SO medium (15) on a 14:10 light dark cycle. Frozen pellets were resuspended, sonicated, and centrifuged, and supernatants were solvent precipitated at −20 °C. Precipitated protein was resuspended, reduced, alkylated, and trypsin-digested. The whole cell lysate digests were analyzed using by liquid chromatography mass spectrometry (LC-MS) using a Paradigm MS4 HPLC system with reverse phase chromatography, a Michrom ADVANCE source, and a Thermo LTQ ion trap mass spectrometer. Two-dimensional chromatography involved adding an offline strong cation exchange separation using a salt gradient prior to reverse phase separation. Nine specific peptides were selected for quantitative analyses via selected reaction monitoring (SRM). Known amounts of heavy labeled versions of each peptide of interest (AQUA peptides; Sigma) were added as internal standards to *Crocosphaera* peptide extracts and analyzed using a Thermo Vantage TSQ Triple Quadrupole Mass Spectrometer with the LC and source as described for the LTQ. Peptide standard sequences and transition information are listed in Table S2. Linear Ion Trap mass spectra were processed using SEQUEST and PeptideProphet, and spectral counts were tabulated in Scaffold 2.0, with a false positive rate of less than 1% (31). Numerical simulations used the MIT general circulation model (MITgcm). The physical circulation flow fields and diffusion, constrained by observations (47), transport the organic and inorganic components of the ecosystem model. The ecosystem model was adapted from Monteiro et al. (10) and includes several types of autotrophs including several nondiazotrophs (analogs of diatoms, other large eukaryotes, *Prochlorococcus*, and other small

ENVIRONMENTAL SCIENCES

phytoplankton) and three types of diazotrophs (analogs of *Trichodesmium*, *Crocosphaera*, and a hypothetic control group of unicellulars that could not share cellular iron between photosynthesis and nitrogen fixation machinery). Other abundant groups of marine diazotroph groups (3) such as *Richelia* sp. symbionts found inside the diatom *Rhizosolenia* spp. and the uncultivated unicellular group A (UCYN-A) are not represented in this study due to lack of information on their iron requirements (4, 44).

1. Falkowski PG (1997) Evolution of the nitrogen cycle and its influence on the biological sequestration of $CO_2$ in the ocean. *Nature* 387:272–274.
2. Moore JK, Doney SC, Lindsay K (2004) Upper ocean ecosystem dynamics and iron cycling in a global three-dimensional model. *Global Biogeochem Cy* 18:10.1029/2004GB002220.
3. Church MJ, Björkman KM, Karl DM, Saito MA, Zehr JP (2008) Regional distributions of nitrogen fixing bacteria in the Pacific Ocean. *Limnol Oceanogr* 53:63–77.
4. Moisander PH, et al. (2010) Unicellular cyanobacterial distributions broaded the oceanic $N_2$ fixation domain. *Science* 327:1512–1514.
5. Montoya JP, et al. (2004) High rates of $N_2$ fixation by unicellular diazotrophs in the oligotrophic Pacific Ocean. *Nature* 430:1027–1032.
6. Zehr JP, et al. (2001) Unicellular cyanobacteria fix $N_2$ in the subtropical North Pacific Ocean. *Nature* 412:635–638.
7. Howard JB, Rees DC (1996) Structural basis of biological nitrogen fixation. *Chem Rev* 96:2965–2982.
8. Rubio LM, Ludden PW (2008) Biosynthesis of the iron molybdenum cofactor of nitrogenase. *Annu Rev Microbiol* 62:93–111.
9. Moore CM, et al. (2009) Large-scale distribution of Atlantic nitrogen fixation controlled by iron availability. *Nat Geosci* 2:867–871.
10. Monteiro F, Follows MJ, Dutkiewicz S (2010) Distribution of diverse diverse nitrogen fixers in the global ocean. *Global Biogeochem Cy* 24:10.1029/2009GB003731.
11. Mills MM, Ridame C, Davey M, Roche JL, Geider RJ (2004) Iron and phosphorus co-limit nitrogen fixation in the eastern Tropical Atlantic. *Nature* 429:292–294.
12. Castruita M, et al. (2006) Overexpression and characterization of an iron storage and DNA-binding Dps protein from *Trichodesmium erythraeum*. *Appl Environ Microbiol* 72:2918–2924.
13. Kustka A, Sanudo-Wilhelmy S, Carpenter EJ, Capone DG, Raven JA (2003) A revised estimate of the iron use efficiency of nitrogen fixation, with special reference to the marine cyanobacterium *Trichodesmium* spp. (Cyanophyta). *J Phycol* 39:12–25.
14. Kustka A, Sanudo-Wilhelmy SA, Carpenter EJ (2003) Iron requirements for dinitrogen- and ammonium-supported growth in cultures of *Trichodesium (IMS 101)*: Comparison with nitrogen fixation rates and iron:carbon ratios of field populations. *Limnol Oceanogr* 48:1869–1884.
15. Tuit C, Waterbury J, Ravizza G (2004) Diel variation of molybdenum and iron in marine diazotrophic cyanobacteria. *Limnol Oceanogr* 49:978–990.
16. Berman-Frank I, Cullen JT, Shaked Y, Sherrell RM, Falkowski PG (2001) Iron availability, cellular iron quotas, and nitrogen fixation in *Trichodesmium*. *Limnol Oceanogr* 46:1249–1260.
17. Shi T, Sun Y, Falkowski PG (2007) Effects of iron limitation on the expression of metabolic genes in the marine cyanobacterium *Trichodesmium erythraeum* IMS101. *Environ Microbiol* 9:2945–2956.
18. Raven JA (1988) The iron and molybdenum use efficiencies of plant growth with different energy, carbon, and nitrogen sources. *Plant Phytol* 109:279–287.
19. Compaoré J, Stal LJ (2009) Oxygen and the light-dark cycle of nitrogenase activity in two unicellular cyanobacteria. *Environ Microbiol* 12:54–62.
20. Schneegurt MA, Sherman DM, Nayar S, Sherman LA (1994) Oscillating behavior of carbohydrate granule formation and dinitrogen fixation in the cyanobacterium *Cyanothece* sp. strain ATCC 51142. *J Bacteriol* 176:1586–1597.
21. Shi T, Ilikchyan I, Rabouille S, Zehr JP (2010) Genome-wide analysis of diel gene expression in the unicellular $N_2$-fixing cyanobacterium *Crocosphaera watsonii* WH 8501. *ISME J* 4:621–632.
22. Stockel J, et al. (2008) Global transcriptomic analysis of *Cyanothece* 51142 reveals robust diurnal oscillation of central metabolic processes. *Proc Natl Acad Sci USA* 105:6156–6161.
23. Reade JPH, Dougherty LJ, Rogers LJ, Gallon JR (1999) Synthesis and proteolytic degradation of nitrogenase in cultures of the unicellular cyanobacterium *Gloeothece* strain ATCC 27152. *Microbiology* 145:1749–1758.
24. Steunou A-S, et al. (2006) In situ analysis of nitrogen fixation and metabolic switching in unicellular thermophilic cyanobacteria inhabiting hot spring microbial mats. *Proc Nat Acad Sci USA* 103:2398–2403.
25. Mohr W, Intermaggio MP, LaRoche J (2009) Diel rhythm of nitrogen and carbon metabolism in the unicellular, diazotrophic cyanobacterium *Crocosphaera watsonii* WH8501. *Environ Microbiol* 12:412–421.
26. Xia Q, et al. (2006) Quantitative proteomics of the archaeon *Methanococcus maripaludis* validated by microarray analysis and real time PCR. *Mol Cell Proteomics* 5:868–881.
27. Malmstrom J, et al. (2009) Proteome-wide cellular protein concentrations of the human pathogen *Leptospira interrogans*. *Nature* 460:762–765.
28. Sowell SM, et al. (2008) Proteomic analysis of stationary phase in the marine bacterium *Candidatus Pelagibacter ubique*. *Appl Environ Microbiol* 74:4091–4100.
29. Ram RJ, et al. (2005) Community proteomics of a natural microbial biofilm. *Science* 308:1915–1920.
30. Sowell SM, et al. (2008) Transport functions dominate the SAR11 metaproteome at low-nutrient extremes in the Sargasso Sea. *ISME J* 3:93–105.
31. Peng J, Elias JE, Thoreen CC, Licklider LJ, Gygi SP (2003) Evaluation of multidimensional chromatography coupled with tandem mass spectrometry (LC/LC-MS/MS) for large-scale protein analysis: The yeast proteome. *J Proteome Res* 2:43–50.
32. Toepel J, Welsh E, Summerfield TC, Pakrasi HB, Sherman LA (2008) Differential transcriptional analysis of the cyanobacterium *Cyanothece* sp. strain ATCC 51142 during light-dark and continuous-light Growth. *J Bacteriol* 190:3904–3913.
33. Schindelin H, Kisker C, Schlessman JL, Howard JB, Rees DC (1997) Structure of ADP x AIF4(-)-stabilized nitrogenase complex and its implications for signal transduction. *Nature* 387:370–376.
34. Erdner DL, Anderson DM (1999) Ferredoxin and flavodoxin as biochemical indicators of iron limitation during open-ocean iron enrichment. *Limnol Oceanogr* 44:1609–1615.
35. Fillat MF, Sandmann G, Gomez-Moreno C (1988) Flavodoxin from the nitrogen-fixingcyanobacterium *Anabaena* PCC 7119. *Arch Microbiol* 150:160–164.
36. Webb EA, Ehrenreich IM, Brown SL, Valois FW, Waterbury JB (2009) Phenotypic and genotypic characterization of multiple strains of the diazotrophic cyanobacterium, *Crocosphaera watsonii*, isolated from the open ocean. *Environ Microbiol* 11:338–348.
37. Church MJ, Short CM, Jenkins BD, Karl DM, Zehr JP (2005) Temporal patterns of nitrogenase gene (nifH) expression in the oligotrophic North Pacific ocean. *Appl Environ Microbiol* 71:5362–5370.
38. Finzi-Hart JA, et al. (2009) Fixation and fate of C and N in the cyanobacterium *Trichodesmium* using nanometer-scale secondary ion mass spectrometry. *Proc Natl Acad Sci USA* 106:6345–6350.
39. Capone D, Zehr J, Paerl H, Bergman B, Carpenter E (1997) *Trichodesmium*, a globally significant marine cyanobacterium. *Science* 276:1221–1229.
40. Weber L, Volker C, Oschlies A, Burchard H (2007) Iron profiles and speciation of the upper water column at the Bermuda Atlantic time-series study site: A model based sensitivity study. *Biogeosciences* 4:689–706.
41. Rhee G-Y (1978) Effects of N:P atomic ratios and nitrate limitation on algal growth, cell composition, and nitrate uptake. *Limnol Oceanogr* 23:10–25.
42. Follows MJ, Dutkiewicz S, Grant S, Chisholm SW (2007) Emergent biogeography of microbial communities in a model ocean. *Science* 315:1843–1846.
43. Campbell J, Carpenter EJ, Montoya JP, Kustka AB, Capone DG (2005) Picoplankton community structure within and outside a *Trichodesmium* bloom in the southwestern Pacific Ocean. *Vie Milieu* 55:185–195.
44. Zehr JP, et al. (2008) Globally distributed uncultivated oceanic $N_2$-fixing cyanobacteria lack oxygenic photosystem II. *Science* 322:1110–1112.
45. Fu F-X, et al. (2008) Interactions between changing $pCO_2$, $N_2$ fixation, and Fe limitation in the marine unicellular cyanobacterium *Crocosphaera*. *Limnol Oceanogr* 53:2472–2484.
46. Shi D, Xu Y, Hopkinson BM, Morel FMM (2010) Effect of ocean acidification on iron availability to marine phytoplankton. *Science* 327:676–679.
47. Wunsch C, Heimbach P (2006) Estimated decadal changes in the North Atlantic meridional overturning circulation and heat flux 1993–2004. *J Phys Oceanogr* 36:2012–2024.